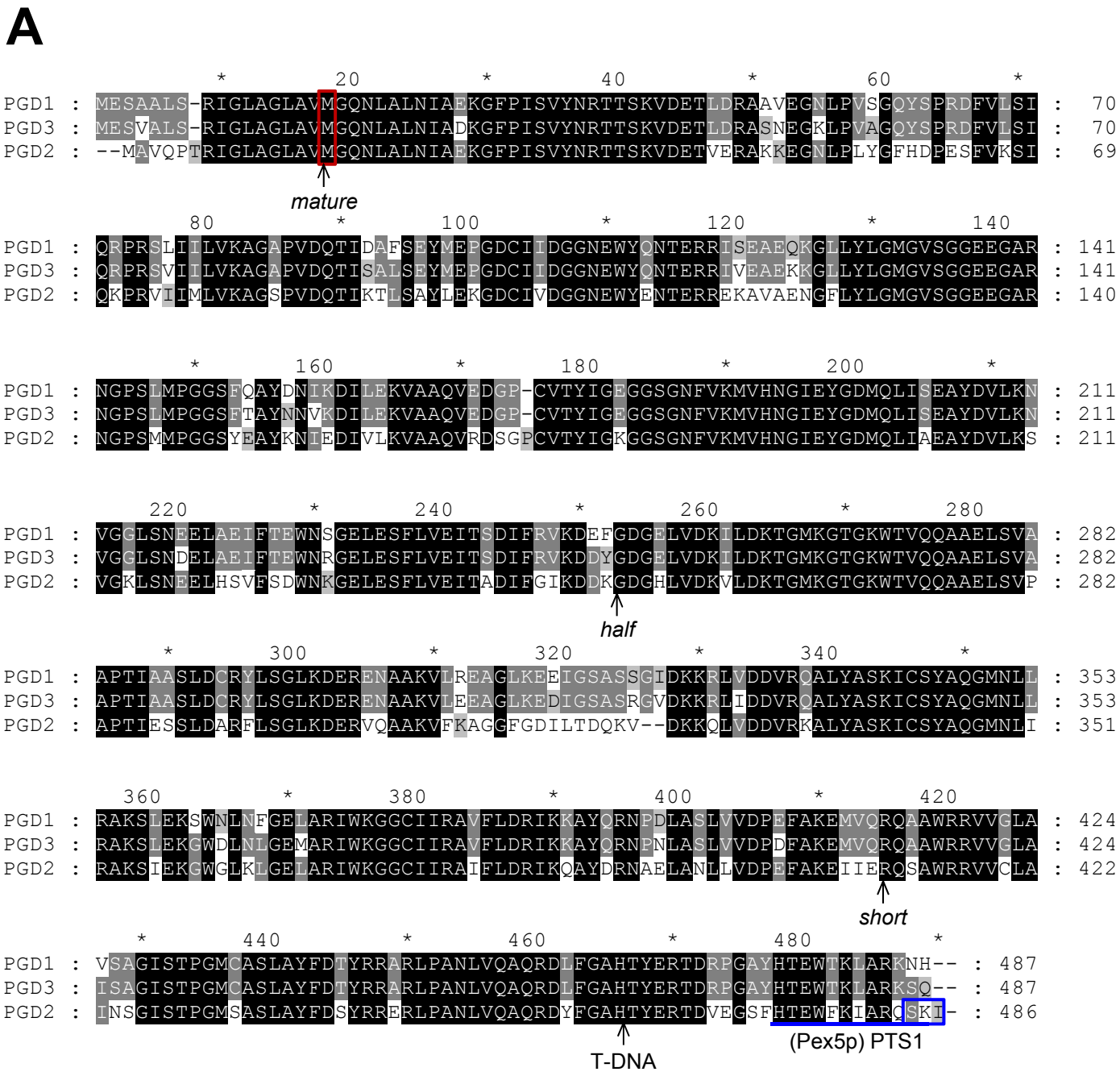

Figure S1A. Amino-acid alignment of PGD polypeptide sequences. **A**) Comparison of the three Arabidopsis PGD isoforms. By contrast to the situation in spinach, none of them carries a N-terminal extension, and PGD2 was previously annotated as cytosolic isoform (Krepinsky et al., 2001). Reporter-fusion and T-DNA insertion sites are marked by upward arrows. The second ATG (M, methionine) in all isoforms is highlighted by a red frame and the C-terminal PTS1 motif of PGD2 (-SKI) by a blue frame (Pex5p-binding site underlined).

B

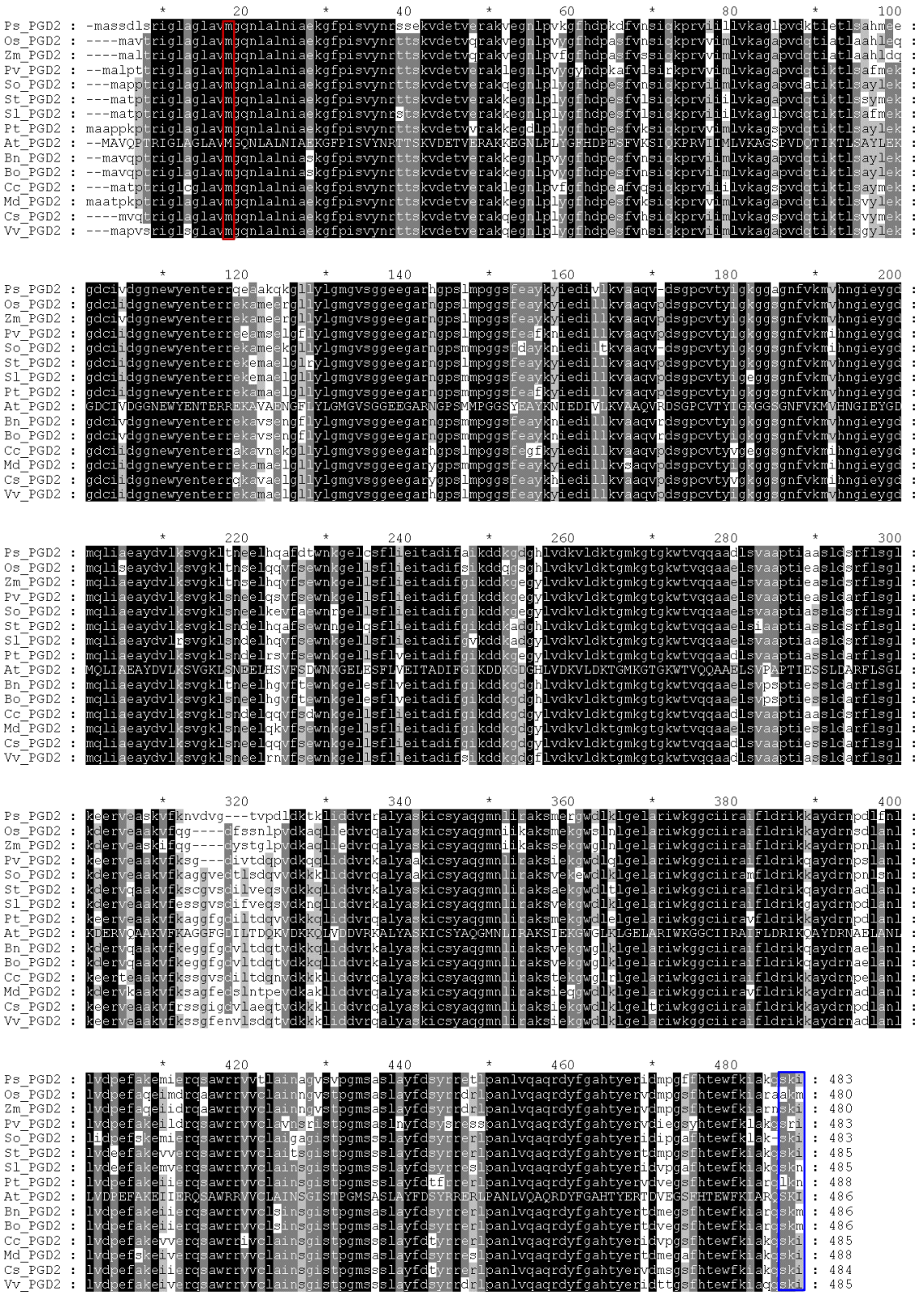

Figure S1B. Alignment of 15 higher plant PGD2 homologs. None of the other Arabidopsis PGD isoforms (PGD1 or PGD3) was obtained upon BLASTp search with At_PGD2 (in capital letters). All PGD2 homologous sequences are absolutely conserved around the second ATG (top, marked red) and terminate with a putative PTS1 motif (bottom, marked blue). Abbreviations: At, *Arabidopsis thaliana*; Bn, *Brassica napus*; Bo, *Brassica oleracea*; Cc, *Coffea canefora*; Cs, *Citrus sinensis*; Md, *Malus domestica*; Ps, *Pinus sylvestris*; Pt, *Populus trichocarpa*; Pv, *Phaseolus vulgaris*; Sl, *Solanum lycopersicum*; So, *Spinacia oleracea*; St, *Solanum tuberosum*; Os, *Oryza sativa*; Vv, *Vitis vinifera*; Zm, *Zea mays*. Identical residues in black, descending similarities in dark to light grey setting.

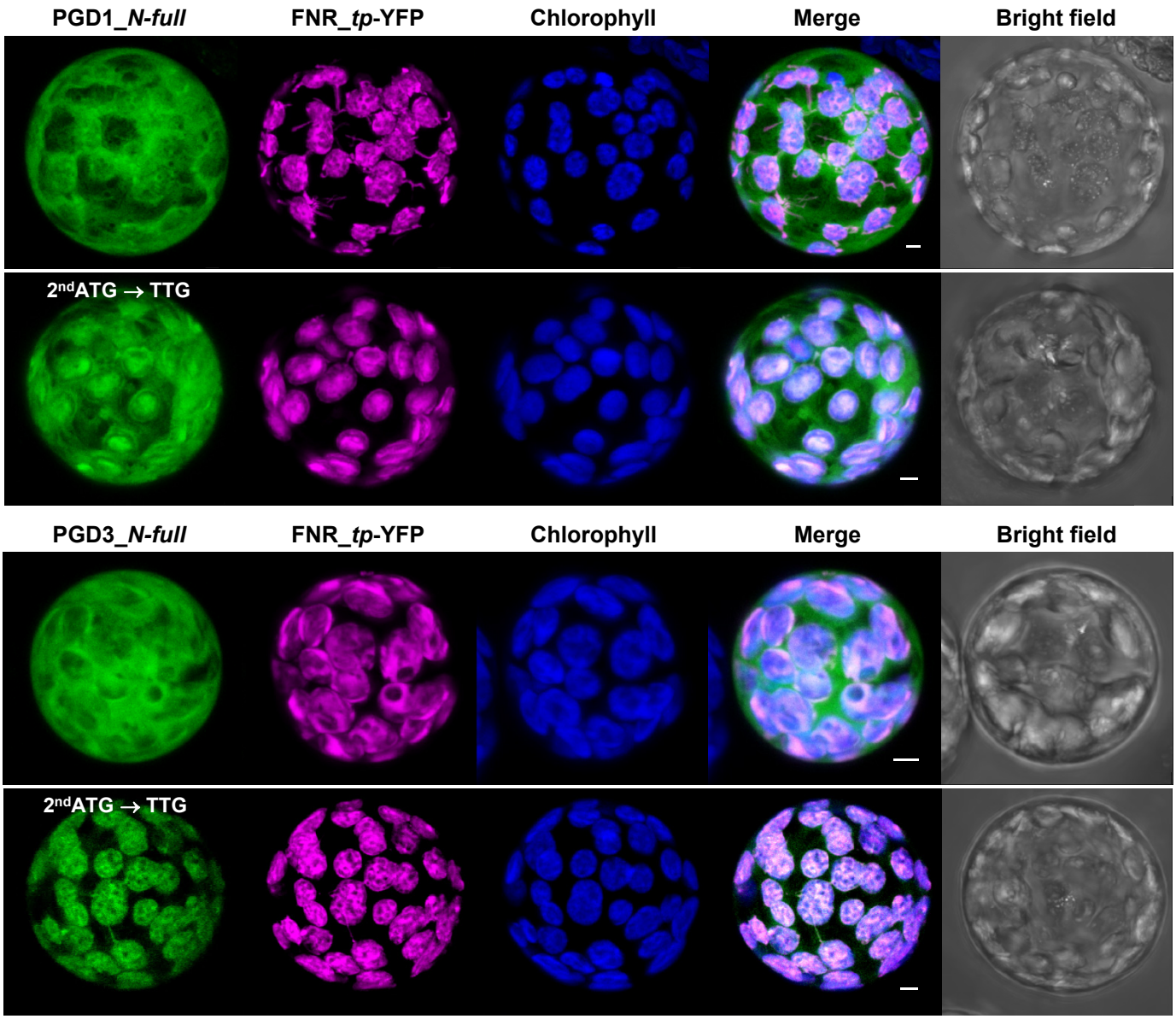

Figure S2. Details of *full-length* PGD1- and PGD3-OFP fusions in tobacco protoplasts (48 h post transfection). The top panels show that the wild-type fusions accumulate in both cytosol and chloroplasts as confirmed by co-localization with a plastidial reporter fusion (transit peptide of ferredoxin-NADP reductase, FNR_*tp*-YFP; magenta). The bottom panels show that upon silent mutagenesis of the second ATG in *PGD1* and *PGD*3, labeling of the cytosol is still observed to various extents. Only maximal projections (of ~35 single sections) are shown. Candidate fusions in green, chloroplast marker (FNR) in magenta, and chlorophyll autofluorescence in blue. Co-localization and very close signals (< 200 nm) appear white in merged images of all channels. Bright field images are shown for reference. Scale bars = 3 µm.

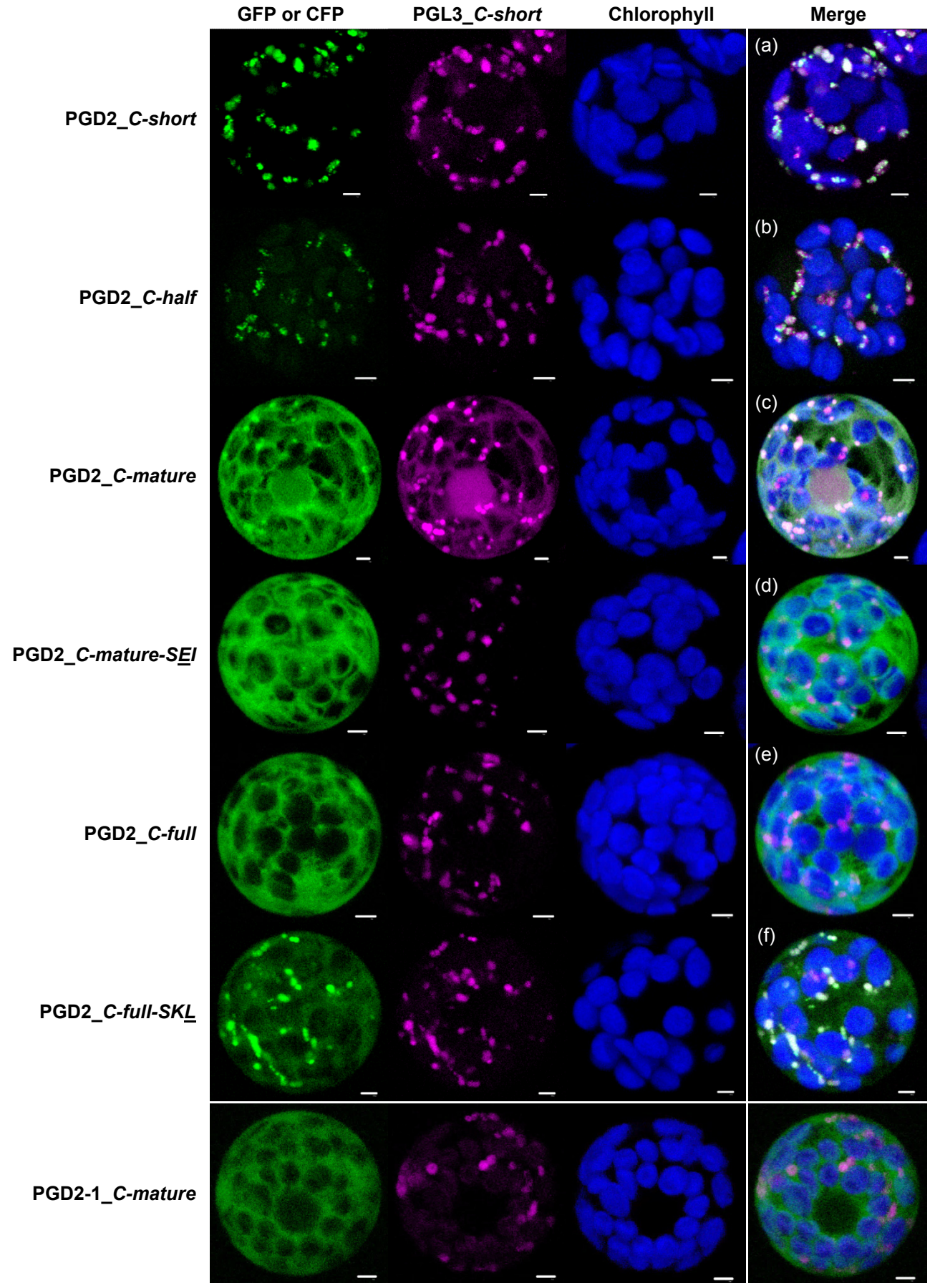

Figure S3. Single channels (left) of merged maximal projections shown in Fig. 2 (a-f) and Fig. 5B (right panels). Candidate fusions in green, peroxisome marker in magenta, and chlorophyll autofluorescence in blue. Co-localization and very close signals (< 200 nm) appear white in merged images of all channels. Scale bars = 3 µm.

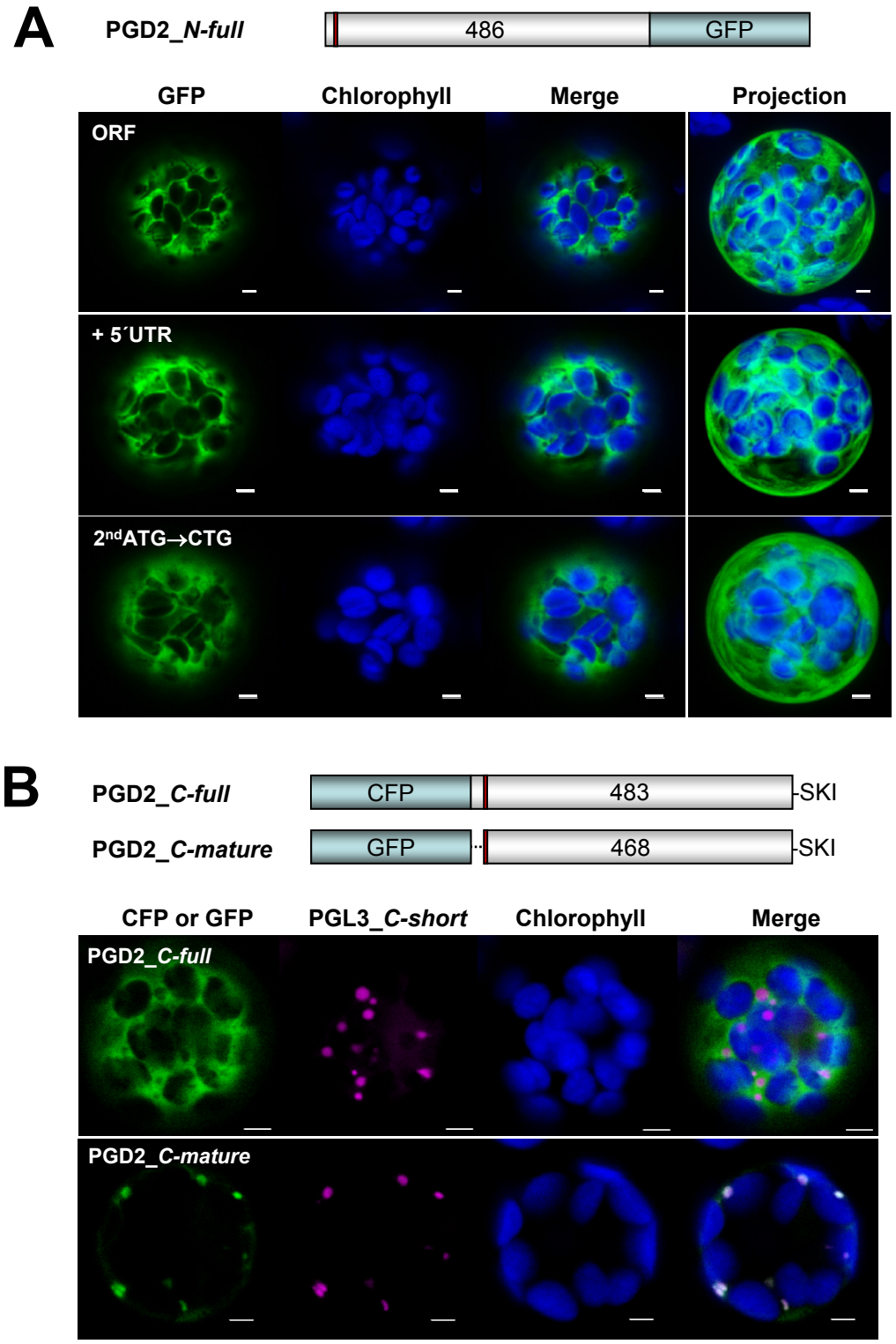

Figure S4. Localization of PGD2-reporter fusions in protoplasts of soil-grown Arabidopsis plants. Protoplasts were swiftly prepared from Arabidopsis leaf tissue, transfected with the indicated fusion constructs, and analyzed 24 h post transfection. **A**) Single sections of representative protoplasts are shown on the left and maximal projections (of ~35 single sections) on the right (compare to tobacco protoplasts in Fig. 1B, panels g-i). **B**) Single sections of co-transfected reporter-*PGD2* fusions (depicted above) with peroxisome marker OFP-PGL3_*C-short*. C/GFP signals in green, OFP signals in magenta, and chlorophyll auto-fluorescence in blue. Co-localization and very close signals (< 200 nm) appear white in merged images of all channels. Scale bars = 3 µm.

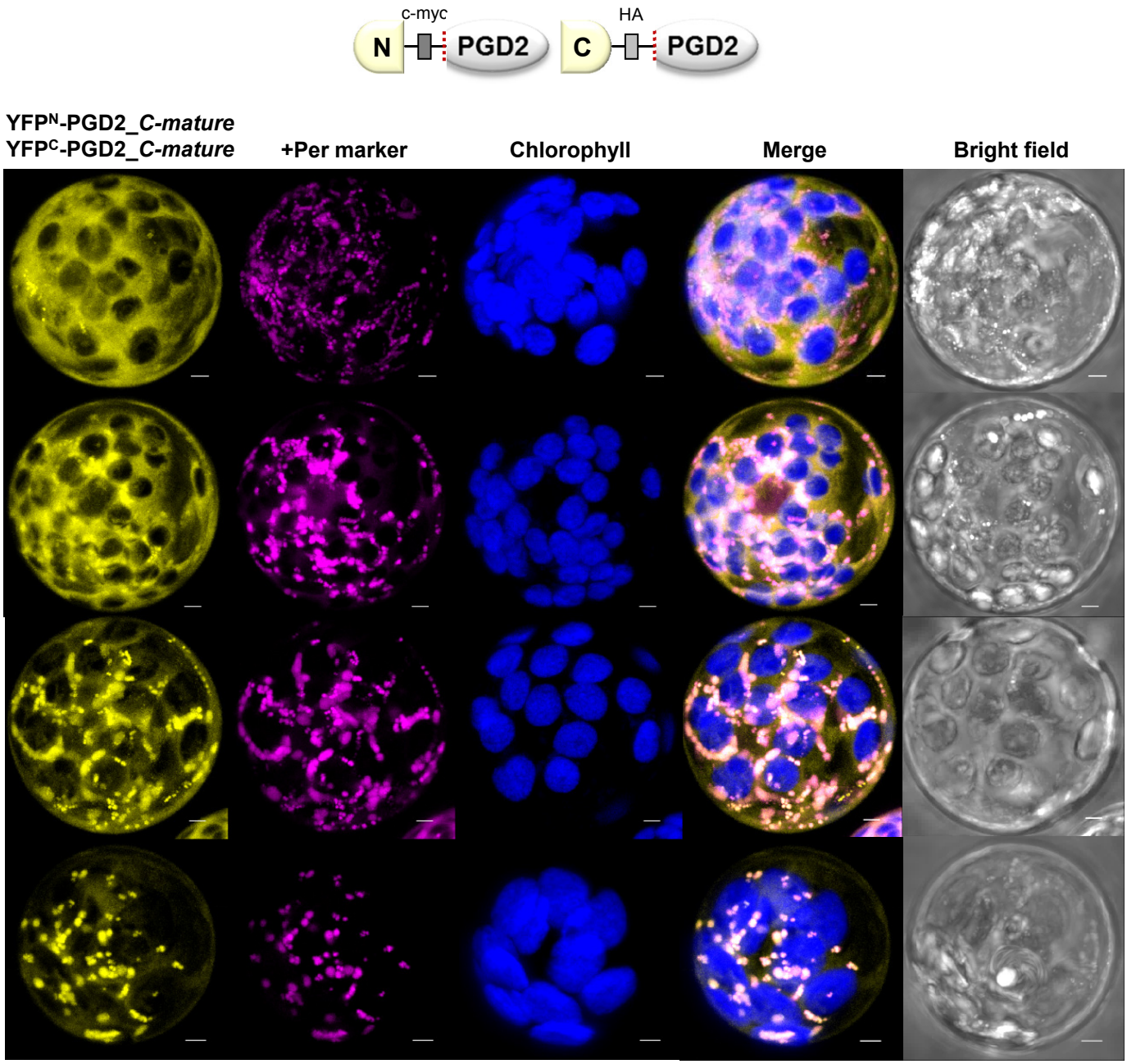

Figure S5. BiFC analyses of PGD2_*C-mature* with free C-terminal ends in Arabidopsis (48 h post transfection). Note that reconstituted YFP signals accumulate first in the cytosol (different cells of the same sample), before labeling mostly peroxisomes (compare Fig. 3, panel h). Only maximal projections (of ~35 single sections) are shown. YFP signals in yellow, peroxisome marker OFP-PGL3_*C-short* in magenta, and chlorophyll autofluorescence in blue. Co-localization and very close signals (< 200 nm) appear white in merged images of all channels. Bright filed images are shown for reference. Scale bars = 3 µm.

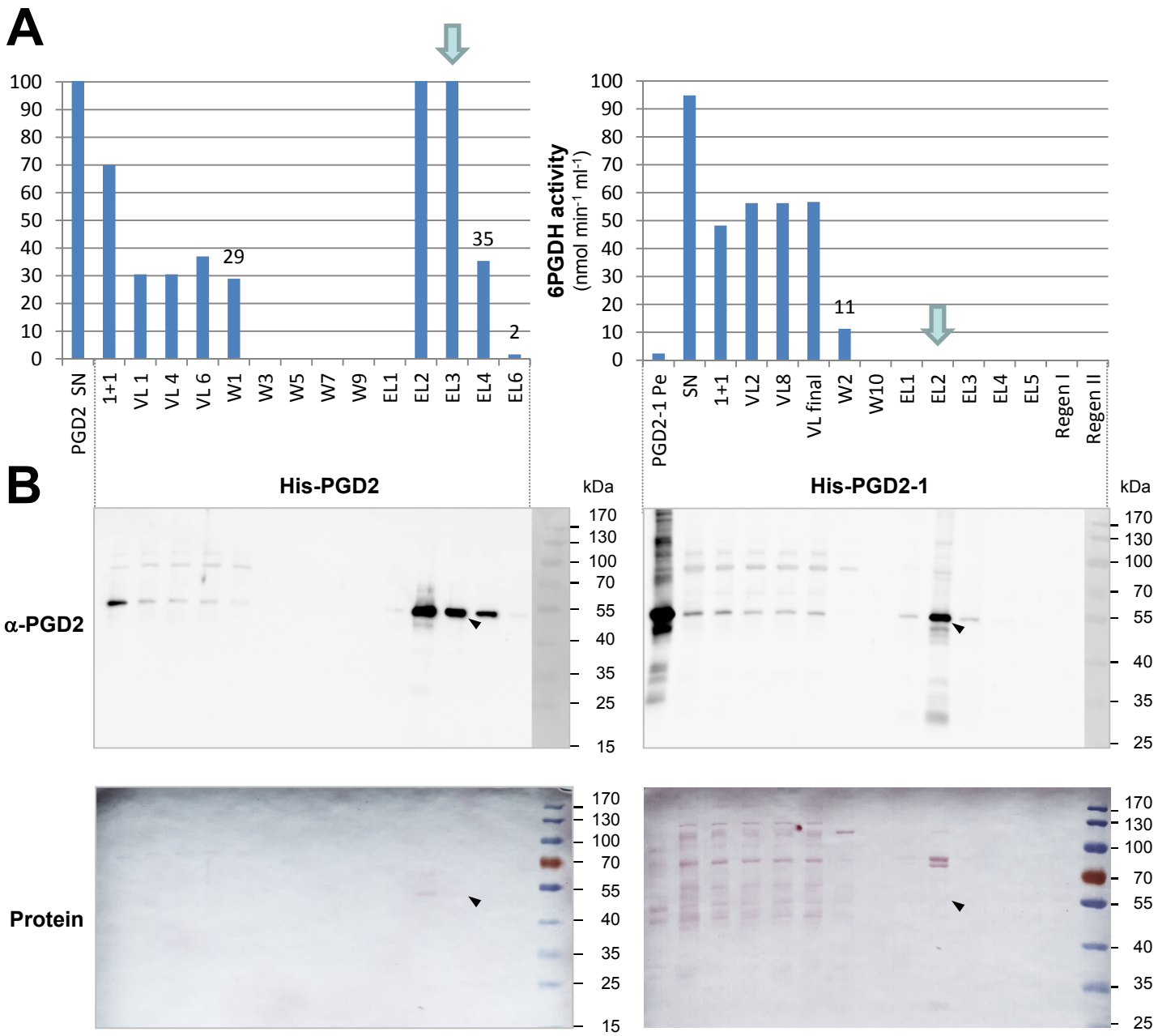

Figure S6. Ni-NTA purification of His-PGD2 and His-PGD2-1. **A**) Upon overexpression in *E. coli* BL21^{minus} (representative experiment), cells were lysed by sonication and centrifuged, resulting in pellet (Pe) and supernatant (SN) fractions. The SN was diluted (1+1) prior to loading on equilibrated Ni-NTA columns (Qiagen). 6PGDH activity (nmol per min and ml) was determined in SN, (Pe), void (VL), wash (W), and elution (EL) fractions before column regeneration. Volume equivalents (10 µl) were subjected to SDS-PAGE and Western blot analysis. **B**) Immunoblot of above indicated Ni-NTA fractions developed with a polyclonal rabbit antiserum raised against denatured His-PGD2. The Ponceau S-stained membrane is shown below as protein loading reference. Molecular masses (kDa) indicated on the right. Arrows mark fractions used for the blot shown in Fig. 5C.

Tetrad analysis with Arabidopsis *quartet* (*qrt*) mutants (Preuss et al., 1994)

QRT1 = Pectinmethylesterase (At5g55590)
QRT2 = Polygalacturonase (At3g07970)
QRT3 = Polygalacturonase (At4g20050)

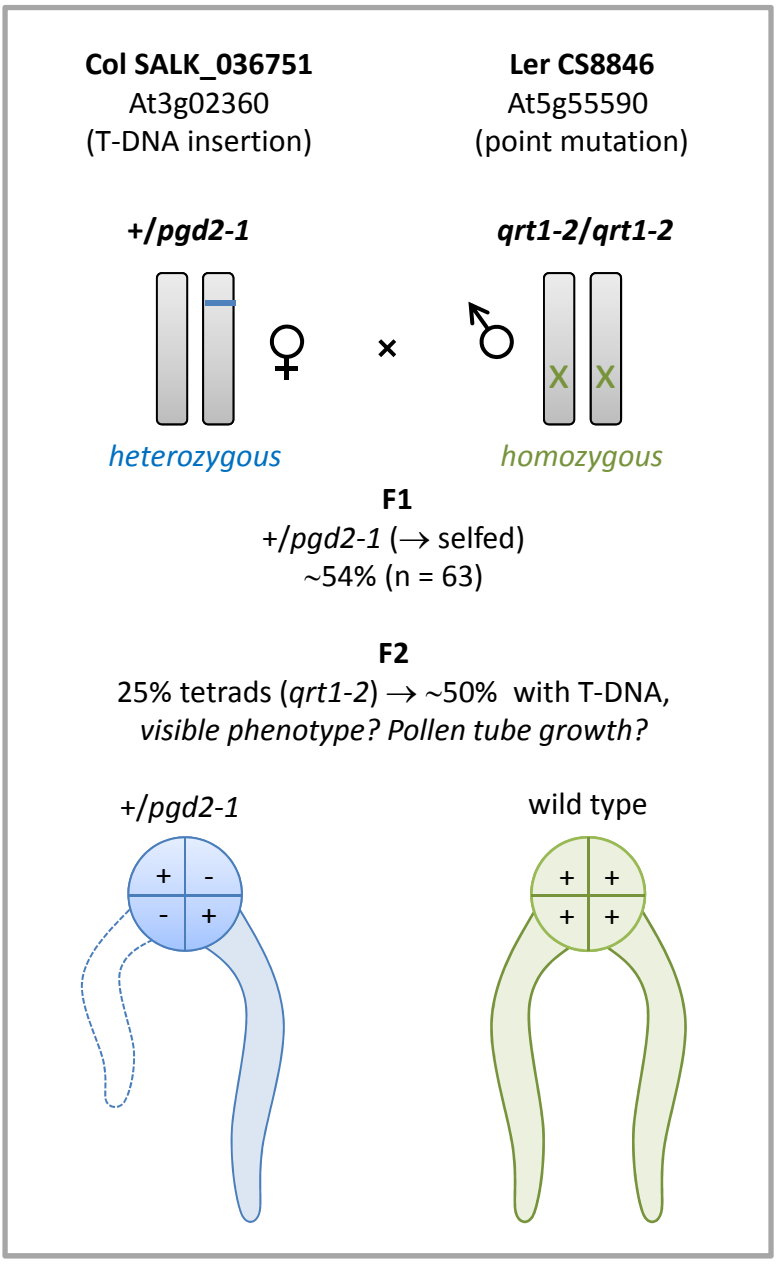

Figure S7. Scheme of *pgd2-1* analyses in the *qrt1-2* background. The Arabidopsis lines used are indicated on top. Plus signs indicate wild-type and minus signs mutant alleles. Presumed defects in pollen-tube growth of the mutant allele is indicated by shorter length and a dashed line (reduced male transmission).

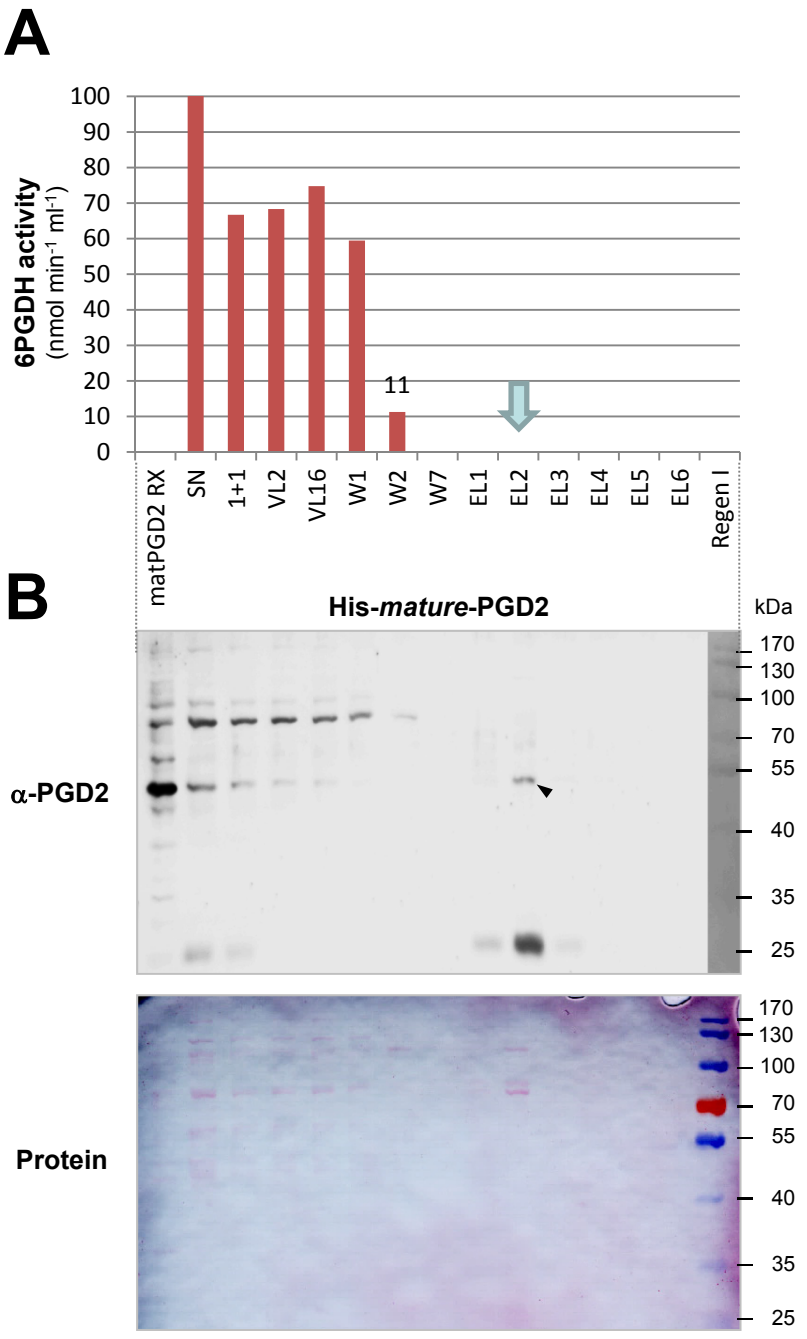

Figure S8. Ni-NTA purification of His-*mature*-PGD2. **A**) Upon overexpression in *E. coli* BL21^{minus} (representative experiment), cells were lysed by sonication and the crude extract (RX) was centrifuged. The supernatant fraction (SN) was diluted (1+1) prior to loading on an equilibrated Ni-NTA column (Qiagen). 6PGDH activity (nmol per min and ml) was determined in RX, SN, void (VL), wash (W), and elution (EL) fractions prior to column regeneration (Regen). Equal volume equivalents (10 µl) were subjected to SDS-PAGE and Western blot analysis. **B**) Immunoblot of the Ni-NTA fractions developed with a polyclonal rabbit antiserum raised against denatured His-PGD2. The Ponceau S-stained membrane is shown as protein loading reference. Molecular masses (kDa) are indicated on the right. The arrow head marks a protein band of correct size in elution fraction EL2, lacking enzymatic activity (panel A).

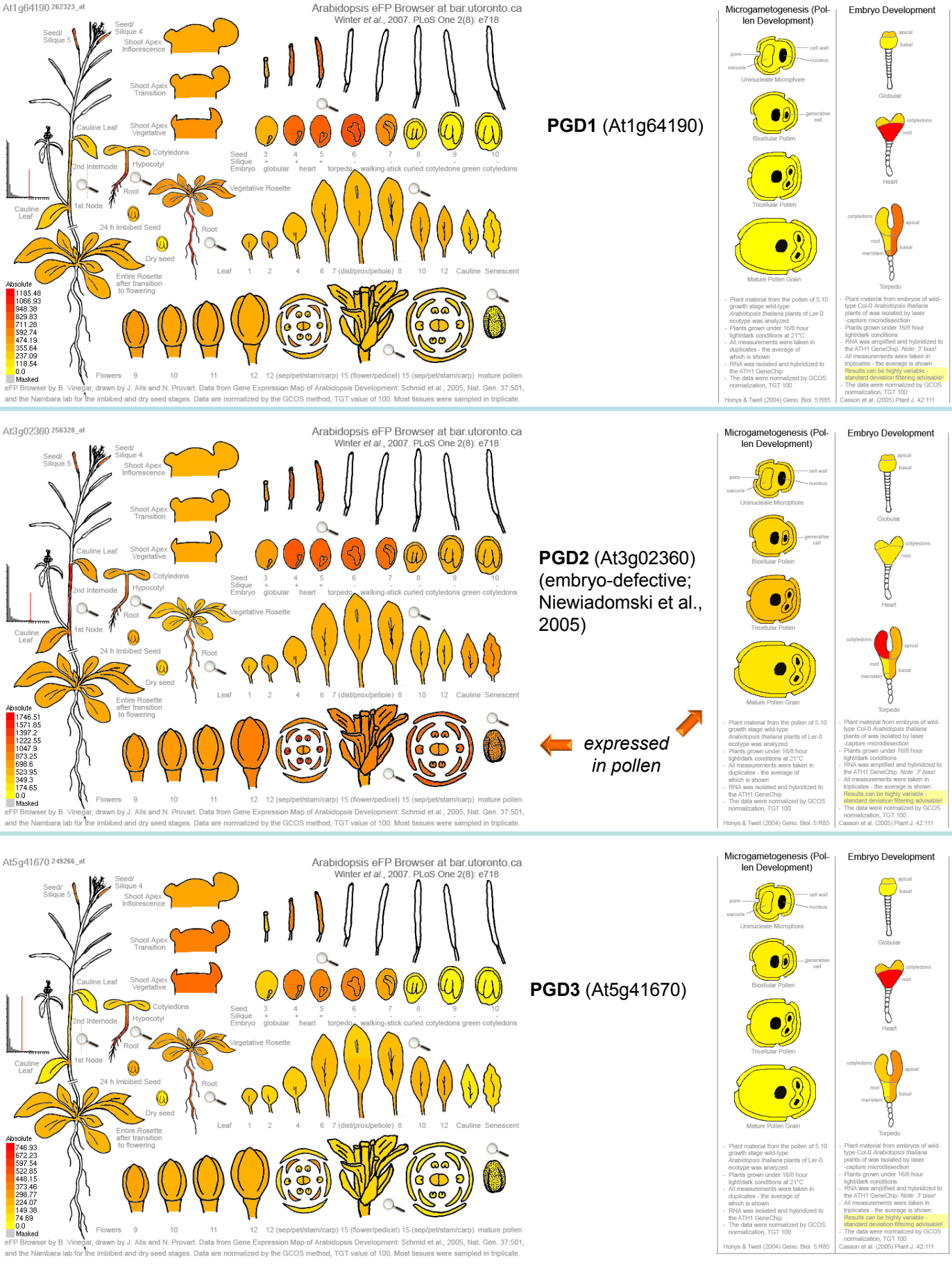

Figure S9. Relevant mRNA Expression patterns of the three Arabidopsis *PGD* isoforms as listed by the BAR eFP browser. Note that peroxisomal isoform *PGD2* is highly expressed in pollen, but also during embryo development.

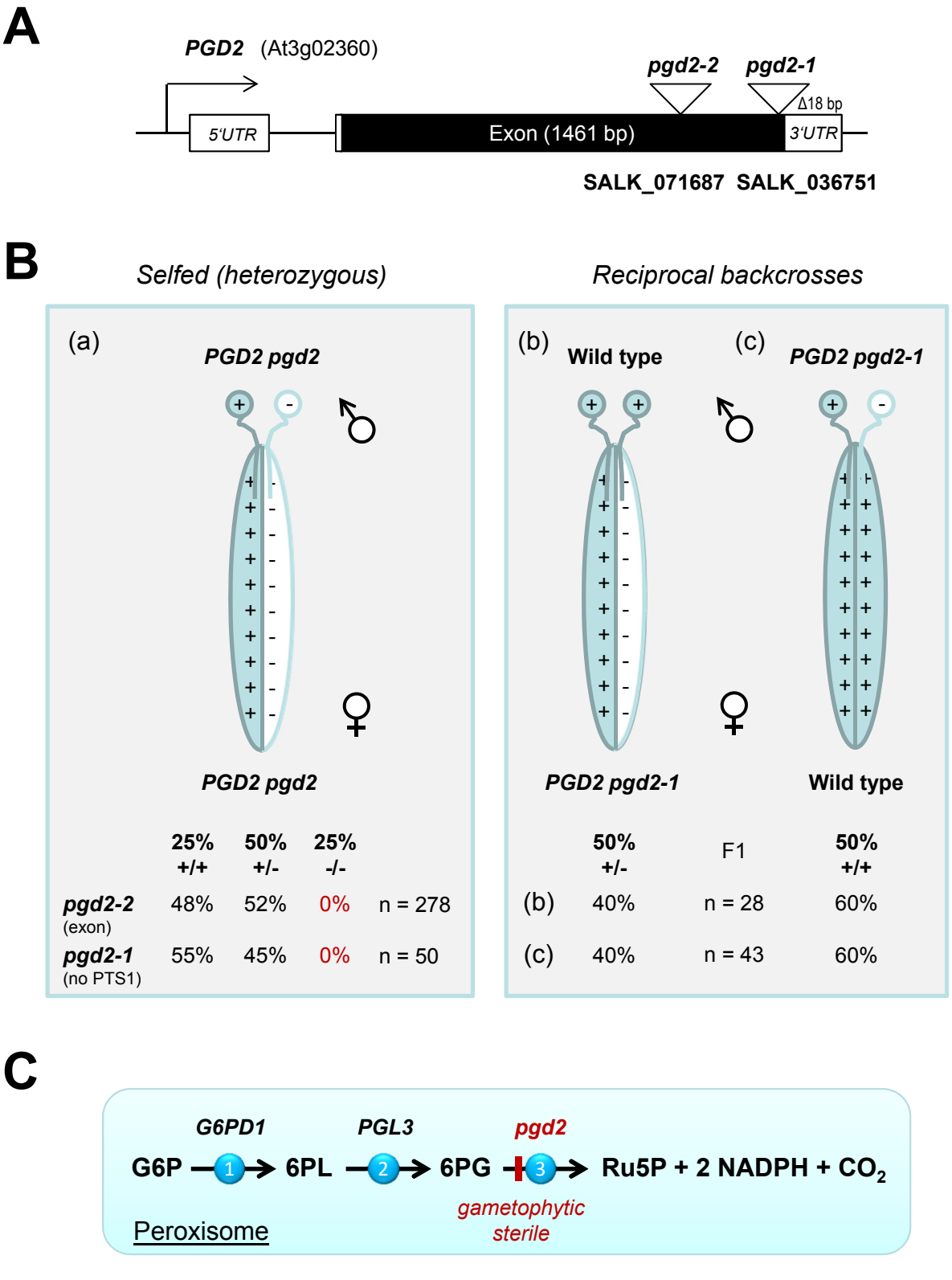

Figure S10. Summary *of PGD2 pgd2* selfing and reciprocal backcrosses. **A**) Scheme of the *PGD2* locus with T-DNA alleles *pgd2-1* and *pgd2-2* (triangles). **B**) Schemes with male (pollen tubes) and female (styles) combinations and percent share of expected and resulting wildtype (+, PGD2) or mutant (-, *pgd2*) allele combinations upon selfing (panel a, left) and reciprocal backcrosses (panels b and c, right). **C**) Scheme of the *pgd2* block in the peroxisomal OPPP branch resulting in gametophytic sterility (the isoforms catalyzing the numbered steps in *Arabidopsis thaliana* are indicated above). Abbreviations: 6PL, 6-phosphogluconolactone; 6PG, 6-phosphogluconate; Ru5P, ribulose 5-phosphate.

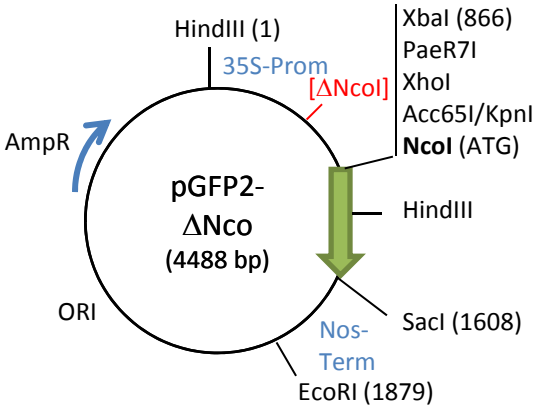

pGFP-2 (B. Kost) →
pGFP2-ΔNco (*sdm*, S. Rips)
(NcoI site in 35S removed, GFP with stop)

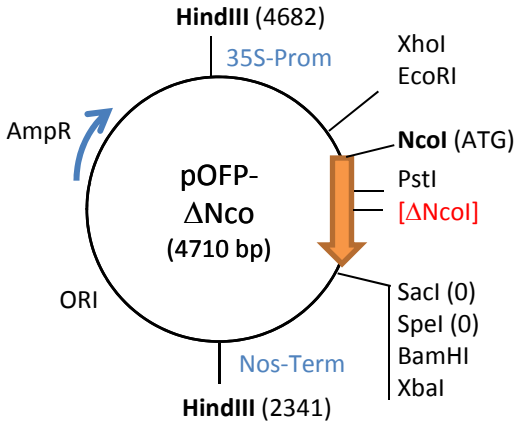

p*m*RFP (pSY526, S. Yalovsky) →
pOFP-ΔNco (*sdm*, T. Meyer)
(silent *sdm* of NcoI site in *m*RFP, OFP with stop)

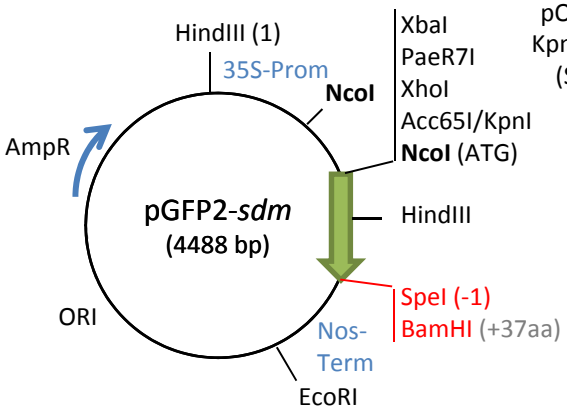

pGFP-2 (B. Kost) →
pGFP2-*sdm* (C. Schwöppe)
(SacI changed to SpeI/BamHI, GFP w/o stop)

OFP via PCR from pOFP-ΔNco with KpnI (NcoI) & SpeI (SacI) primers

NcoI *sdm*, reporter re-insertion after PCR via XbaI/BamHI

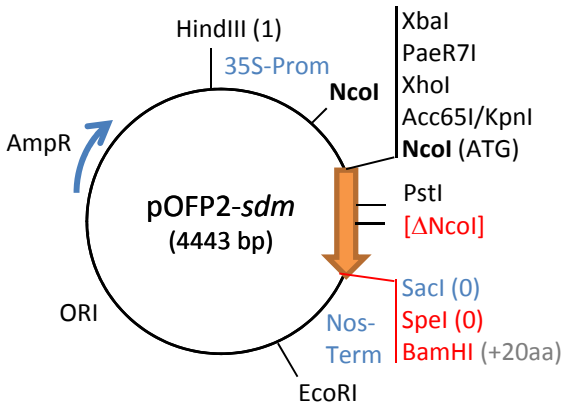

pGFP2-*sdm* (S. Rips) →
pOFP2-*sdm* (A. Stirnberg)
(reporter exchanged, OFP w/o stop)

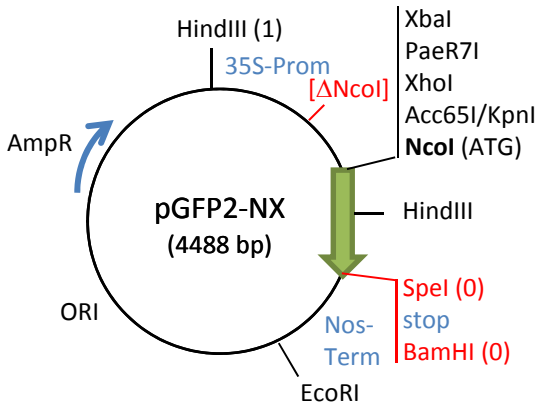

pGFP2-*sdm* →
pGFP2-NX (H. Lansing)
(ΔNco via *sdm,* GFP with stop between SpeI/BamHI)

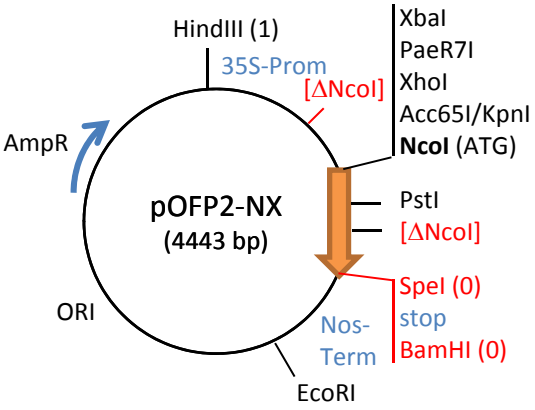

pOFP2-*sdm* →
pOFP2-NX (H. Lansing)
(ΔNco via *sdm,* OFP with stop between SpeI/BamHI)

Figure S11. Cloning *s*cheme of the new pG/OFP-NX vectors. For source and cloning of other reporter vectors, compare our previous publications (Frank et al., 2008; Meyer et al., 2011; Hölscher et al., 2014).